Predicted Performance of InP Solar Cells in Cassegrainian and Slats Space Concentrator Arrays at 20 to 100 AM0, 80° to 100°C

Chandra Goradia, William Thesling and Manju Ghalla Goradia
Electrical Engineering Department
Cleveland State University
Cleveland, Ohio 44115

Irving Weinberg, Clifford K. Swartz
NASA Lewis Research Center
Cleveland, Ohio 44135

Summary

We have calculated the expected performance dependence of near-optimally designed shallow homojunction n^+pp^+ InP solar cells on incident intensities up 200 AM0 and temperatures up to 100°C (373K). Both circular and rectangular cells have been considered, the former for use in a Cassegrainian concentrator array at 100 AM0, 80°-100°C and the latter for use in a Slats type concentrator array at 20 AM0, 80°-100°C. Calculation of the temperature dependence of the performance parameters I_{sc}, V_{oc}, FF and η was done by first verifying that the use of the measured temperature variation of I_{sc}, of the best published value of the temperature dependence of the bandgap of InP, and of the temperature dependences of the lifetimes and mobilities of electrons and holes the same as in equivalently doped GaAs, gave calculated results that closely matched measured data on the temperature variation of I_{sc}, V_{oc} and FF of four existing InP cells at 1 AM0. It was then assumed that the same temperature dependences of I_{sc}, the bandgap and lifetimes and mobilities would hold in the near-optimally designed cells at the higher concentrations.

Introduction

Designs already exist for Cassegrainian [ref. 1] and Slats [ref. 2] lightweight space concentrator arrays for use with high efficiency GaAs solar cells [ref. 3] of geometries and dimensions shown in Fig. 1. Also indicated in this figure are the design operating points of 100 AM0, 80°C, with total illuminated area (also cell area) of a 4 mm diameter circle for the Cassegrainian concentrator and 20 AM0, 80°C, with total illuminated and cell area of a 2.5 mm × 1 cm rectangle for the Slats or Venetian Blind concentrator. Note that practical considerations of minimizing payload weight in space require that the cells be operated at the somewhat higher temperatures of 80°C to 100°C.

In an earlier paper [ref. 3], we had predicted the performance of near-optimum GaAs solar cells at 100 and 20 AM0, 80°C when used in these concentrator arrays. Because of the superior radiation tolerance behavior of InP solar cells in comparison to GaAs cells, there is now interest in predicting the performance of near-optimally designed InP space solar cells at 100 and 20 AM0, 80°C to 100°C for use in these same concentrator arrays.

The problem with predicting the performance of near-optimally designed InP solar cells at 100 AM0 and 20 AM0, 80°C to 100°C is that there are no reliable data in the published literature on the temperature variations of such fundamental parameters as the bandgap, optical absorption coefficient, and electron and hole mobilities and lifetimes in both n-type and p-type InP with various doping concentrations. Thus, while our rather comprehensive computer simulation model is capable of predicting the performance and thereby generating a near-optimum design of the InP cell at 100 AM0 and 20 AM0, 27°C (300K), it cannot predict the performance at 80° C to 100°C. We therefore went around this problem using the following multistep approach.

To begin with, we generated near-optimum designs for both the circular and rectangular cells for operation at 100 AM0 and 20 AM0, respectively, at 27°C (300K). This was done with the help of our simulation model, the details about which have been published earlier [ref. 4]. Next, we measured the temperature dependences of the performance parameters I_{sc}, V_{oc} and FF at 1 AM0 for four InP shallow homojunction solar cells. Figure 2 shows these temperature dependences for one typical cell. Then, using a two-diode model,

$$I = I_{ph} - I_{01}[\exp((V + IR_s)/V_T) - 1] - I_{02}[\exp((V + IR_s)/2V_T) - 1] - (V + IR_s)/R_{sh},$$

we obtained, for each of the four cells, all the unknowns of this model at 300K, namely, I_{ph}, I_{01}, I_{02}, R_s and R_{sh} by curve-fitting the above equation to the measured illuminated I-V curve at 300K for each cell. Next, for the temperature variation of I_{ph}, we used the measured temperature variation of I_{sc}. We also used the temperature variation of the bandgap of InP from the published literature and for the temperature dependences of the mobilities and lifetimes, we used those of equivalently doped GaAs. We then calculated I_{sc}, V_{oc} and FF at various temperatures for each of the four cells, using the above-described temperature dependences of the various parameters and found nearly perfect fits to the measured data in the temperature range of 300K to 373K. This indicated to us that the temperature dependences we used for the various parameters must be close to the true temperature dependences of those parameters for InP. As a final step, we then assumed that these same temperature dependences would hold in the near-optimally designed cells not just at 1 AM0 but at the higher intensities of 20 AM0 and 100 AM0. This allowed us to calculate the predicted performance of the near-optimum rectangular and circular cells at 20 AM0, 80°C -100°C and 100 AM0, 80°-100°C respectively. The results of these calculations are presented and discussed in the following section.

Calculated Results and Discussion

Tables 1A and 1B give the general design parameters and the geometrical and material parameters of the near-optimum designs of the rectangular and circular cells. The key points to be noted in these tables are as follows: 1) While we have used a single layer antireflection (AR) coating of 750Å of SiO, we are in the process of incorporating into our model a two-layer ZnS/MgF_2 AR coating which will somewhat boost the short circuit current I_{sc}. 2) A significant portion, nearly 40%, of the total series resistance R_s, which is relatively high, comes from the contact resistance of the front grid fingers; hence, for these concentrator cells, it is imperative that research be done to bring the specific contact resistivity of the front metallization down to about 5E-6 ohm-cm^2. This would raise the fill factor FF slightly. 3) There is some uncertainty in the value of the intrinsic

carrier concentration n_i at 300K; if its value is closer to 1E7 cm^{-3} as some researchers claim, that would boost the expected open circuit voltage V_{oc} by more than 25mV at 300K. 4) The effective front surface recombination velocity (SRV) S_f is an area-weighted average between half the thermal velocity over the area of actual contact of the front grid fingers, which we took as 35% of the grid finger area, and a passivated surface SRV value of 2E4 cm/s over the rest of the area. While this area-weighted average of S_f is believed to be correct for the calculation of the dark or loss current contribution from the emitter, we strongly suspect that it is not correct for the photocurrent contribution from the emitter, for which S_f should be closer to the lower passivated value of 2E4 cm/s. We are in the process of doing calculations with separate values of S_f for the dark and photocurrent contributions from the emitter and these should again boost I_{sc} somewhat. 5) Present experimental results indicate that at 1 AM0, a thinner emitter (~200Å) and a thicker base (~ 3μm) than our values in Table 1B would most probably yield a somewhat higher efficiency [refs. 5,6]. However, we feel that for a concentrator cell, a thinner emitter would require heavier emitter doping to keep the series resistance low and that would add to the uncertainties of any detrimental heavy doping effects. Thus, we have chosen to stay with an emitter thickness of ~400Å. As to the base thickness, radiation damage considerations would favor our thinner base. 6) The effective lifetime values for each region in Table 1B take into account both radiative and Hall-Shockley-Reed recombinations. Auger recombination is insignificant at the low carrier densities and the relatively low tempertures considered.

Table 2 gives the temperture dependence of I_{sc} for the circular cell for various AM0 concentrations. This was based on the average measured temperature dependence of $J_{sc}(T) = 0.030475 + 21.91E\text{-}6 \cdot T$ A/cm^2/AM0 sun obtained from the four measured cells, and the assumption that J_{sc} is a linear function of incident intensity. For the rectangular cell, the I_{sc} values will be proportionally larger in the ratio of the areas of the two cells. It is expected that a two-layer AR coating and a reduced value of S_f for photocurrent in the emitter will boost the 300K value of J_{sc} from its present 36.45 mA/cm^2/AM0 sun to about 40 mA/cm^2/AM0 sun.

Tables 3A and 3B give the V_{oc}, FF and efficiency η as functions of AM0 intensity and temperature for the circular and rectangular cell respectively. Here, the two columns labeled 'Expected' and 'Worst Case' refer to calculations made two different ways. The numbers in the 'Expected' columns were obtained by taking into account the temperature variations of I_{sc}, the bandgap, and mobilities and lifetimes, that is, all parameters that vary with temperature. The numbers in the 'Worst Case' columns were obtained by ignoring the temperature variations of mobilities and lifetimes but taking into account only the temperature variations of I_{sc} and the bandgap. Since 27°C (300K) is the reference temperature, the 'Expected' and 'Worst Case' values coincide at 300K. Figures 3, 4 and 5 give 'expected' and 'worst case' curves of V_{oc}, FF and η as functions of temperature at various AM0 concentrations for both the circular (C) and rectangular (R) cells. It is seen from both the Tables 3A, 3B and Figures 3, 4 and 5, that since the 'worst case' values are so close to the 'expected' values, the primary temperature variation of the performance parameters comes from the variations of I_{sc} and the bandgap with temperature. Actually, since most of the temperature variation of I_{sc} is also due to the temperature variation of the bandgap (and thence of the optical absorption coefficient), the reduction of the bandgap with temperature is the single most important factor contributing to the temperature variation of the performance of the cell.

From Figure 3, it is seen that over the temperature range of interest, 27°C (300K) to 100°C (373K), V_{oc} degrades linearly with increasing temperature. Since fill factor FF is directly dependent on V_{oc}, FF also degrades with increasing temperature, but not quite linearly, as seen in Figure 4. Finally, Figure 5 shows the somewhat nonlinear degradation of the efficiency η with increasing temperature.Note that for both the circular and rectangular cells, the fill factor appears to degrade

monotonically for concentrations above 20 AM0. This is due to the relatively high series resistance for both geometries. If the specific contact resistivity of the front grid fingers can be brought down to about 5E-6 ohm-cm^2 or lower, it may then be possible for the FF to reach its maximum at 100 AM0 or higher instead of at ~20 AM0 as is presently the case. Table 4 gives the rate of degradation with temperature of V_{oc} and η, that is dV_{oc}/dT in mV/°C and $d\eta/dT$ in %/°C, around the nominal operating temperature of 80°C for the circular cell. Note that the magnitudes of dV_{oc}/dT and $d\eta/dT$ decrease with increasing sunlight concentration, as expected. The dV_{oc}/dT is less than 1.75 mV/°C in magnitude for concentrations above 20 AM0. This is between the value for Si (~2.0 mV/°C) and for GaAs (~1.5mV/°C) at 20 AM0 [ref. 3].

Finally, the most important thing to note from Tables 3A, 3B and Figure 5 is that at the nominal operating point of 100 AM0, 80°C, the circular cell is expected to have an efficiency of 21.1%. However, with a two-layer AR coating and a lower S_F for photocurrent from the emitter, a 10% increase in I_{sc} should increase the efficiency to 23.2%, which we think is a realistically achievable efficiency of the circular cell at 100 AM0, 80°C. Similarly, we feel that a realistically achievable efficiency for the rectangular cell at 20 AM0, 80°C is 22.6% instead of the presently predicted 20.57% in Table 3B. These compare very favorably with similar efficiencies predicted for GaAs solar cells [ref. 3].

Concluding Remarks

We may make the following final comments:

1. When reliable data on the temperature dependences of key material parameters such as bandgap, and lifetimes and mobilities of electrons and holes are not available, as is the case with InP, extracting these from a comparison between calculated and measured illuminated I-V curves at several temperatures is a very useful technique. In the case of InP, it turns out that excellent results are obtained by using the published temperature dependence of the bandgap, the measured temperature variation of I_{sc} and the temperature variations of lifetimes and mobilities the same as those in equivalently doped GaAs.

2. The primary temperature dependence of the performance parameters of a solar cell comes from the temperature variation of the bandgap, which causes a temperature variation of I_{sc} through the variation of the optical absorption coefficient and of V_{oc} and FF through the strong temperature dependence of the intrinsic carrier concentration n_i. Thus, as a first approximation, one may even ignore the temperature dependences of lifetimes and mobilities, as we have done to calculate the 'worst case' values.

3. At the design temperature of 80°C, the expected performance of a near-optimum shallow homojunction InP cell is:

	100 AM0 (Circular)	20 AM0 (Rectangular)
J_{sc} A/cm^2	3.821	0.764
V_{oc} mV	946.2	896.8
FF %	81.40	83.72
η %	21.10	20.57

As stated earlier, efficiencies of 23.2% and 22.6%, should be realistically achievable for the circular and rectangular cell respectively, at their design operating points.

4. With efficiencies exceeding 22% at 80° C, 20 AM0 and 100 AM0, both the rectangular and circular InP shallow homojunction solar cells compare very favorably to GaAs cells of the same design and may be preferred in space over the GaAs cells because of the superior radiation tolerance of the InP cells.

References

[1] R. E. Patterson, H. S. Rauschenbach and M. D. Cannady, *Conf. Rec. 16th IEEE PVSC,IEEE Publ. No. 82CH1821-8*, 1982, pp. 39-44.

[2] M. Cornwall et al, Interim Reports from General Dynamics to Air Force Wright Aeronautical Labs. Under Contract No. F-33615-83-C-2319.

[3] C. Goradia, M. Ghalla-Goradia and H. Curtis, *Conf. Rec. 17th IEEE PVSC, IEEE Publ. No. 84CH2019-8*, 1984, pp. 56-62.

[4] C. Goradia, J. Geier, I. Weinberg, *Conf. Rec. 19th IEEE PVSC, IEEE Publ. No. 87CH2400-0*, 1987, pp. 937-943.

[5] C. Keavney, "InP Shallow Homojunction Solar Cells", these Proceedings.

[6] M. Wanlass, T. Gessert, K. Emery, T. Coutts, "Emperical and Theoretical Studies of the Performance of OMCVD InP Homo-junction Solar Cells as a Function of Emitter Thickness and Doping, and Base Doping", these Proceedings.

TABLE 1A

General Cell Parameters of

Near-Optimum Cell Design

	Rectangular	Circular
Total Area A, cm^2	0.25	0.1257
Grid Shadowing	4%	4%
AR Coating	750 Å SiO	750 Å SiO
Specific Contact Resistance R_{ms}, ohm-cm^2		
To n^+ emitter	2E-5	2E-5
To p^+ BSF layer	1E-3	1E-3
Series Resistance R_s, milliohms	59.7	92
Shunt Resistance R_{sh}, ohms	1E7	1E7
Bandgap of InP at 300K, E_g, eV	1.35	1.35
Intrinsic Carrier Concentration n_i at 300K, cm^{-3}	1.65E7	1.65E7
Effective Front SRV S_f, cm/s	1.1E5	1.1E5

TABLE 1B

Geometrical and Material Parameters of Near-Optimum Cell Design

Note: The following parameters are identcal

for both rectangular and circular cells.

Emitter	
Width W_E	0.04 μm(400 Å)
Doping N_{dE}	2E18 cm^{-3}
Effective Lifetime τ_{pE}	1.26 ns
Diffusion Length L_{pE}	0.42 μm
Base	
Width W_B	1.5 μm
Doping N_{aB}	5E16 cm^{-3}
Effective Lifetime τ_n	17.8 ns
Diffusion Length L_{nB}	12.75 μm
BSF Region	
Width W_{BSF}	250 μm
Doping $N_{a,BSF}$	5E18 cm-3
Effective Lifetime $\tau_{n,BSF}$	0.18 ns
Diffusion Length $L_{n,BSF}$	1.06 μm

TABLE 2

Temperature Dependence of I_{SC}

$Jsc(T) = 0.030475 + 21.91E\text{-}6 \bullet T$ $A/cm^2/AMO$ sun

T is in kelvins

At 300K, this gives $J_{SC} = 36.45$ $mA/cm^2/AMO$ sun

AMO Concentration	Short Circuit Current I_{SC}, mA @ 27°C (300K)	@ 80°C (353K)	@ 100°C (373K)
1	4.581	4.8029	4.858
20	91.62	96.058	97.16
100	458.1	480.29	485.8
200	916.2	960.58	971.6

TABLE 3A

Predicted Parameters of Near-Optimum Circular Cell

at 27°C, 80°C and 100°C at 1, 20, 100 and 200 AMO

AMO Concentration	@ 27°C (300K)		@ 80°C(353K)		@ 100°C(373K)	
	Expected	Worst Case	Expected	Worst Case	Expected	Worst Case
			V_{oc} mV			
1	906.4	906.4	802.3	796.6	762.6	754.5
20	987.0	987.0	896.8	891.8	862.4	855.2
100	1029.0	1029.0	946.2	941.2	914.5	907.5
200	1047.0	1047.0	967.4	962.4	936.9	929.9
			FF %			
1	85.14	85.14	82.01	81.76	80.80	80.33
20	86.52	86.52	83.97	83.86	82.90	82.74
100	84.11	84.11	81.40	81.30	80.29	80.15
200	80.65	80.65	77.65	77.54	76.44	76.28
			η %			
1	20.49	20.49	18.04	17.84	17.08	16.80
20	22.67	22.67	20.63	20.49	19.82	19.61
100	22.98	22.98	21.10	20.96	20.35	20.15
200	22.41	22.41	20.57	20.44	19.84	19.66

TABLE 3B

Predicted Parameters of Near-Optimum Retangular Cell

at 27°C, 80°C and 100°C at 1, 20, 100 and 200 AMO

AMO Concentration	@ 27°C (300K)		@ 80°C(353K)		@ 100°C(373K)	
	Expected	Worst Case	Expected	Worst Case	Expected	Worst Case
			V_{oc} mV			
1	906.4	906.4	802.3	796.6	762.6	754.5
20	987.0	987.0	896.8	891.8	862.4	855.2
100	1029.0	1029.0	946.2	941.2	914.5	907.5
200	1047.0	1047.0	967.4	962.4	936.9	929.9
			FF %			
1	85.14	85.14	82.01	81.76	80.80	80.33
20	86.29	86.29	83.72	83.61	82.64	82.47
100	83.01	83.01	80.18	80.08	79.03	78.88
200	78.48	78.48	75.28	75.17	73.99	73.82
			η %			
1	20.49	20.49	18.04	17.84	17.08	16.80
20	22.61	22.61	20.57	20.43	19.75	19.55
100	22.67	22.67	20.78	20.65	20.03	19.84
200	21.81	21.81	19.94	19.81	19.21	19.02

TABLE 4

Temperature Dependence of V_{OC} and η

AMO Concentration	dV_{OC}/dT mV/°C		$d\eta/dT$ %/°C	
	Expected	Worst Case	Expected	Worst Case
20	-1.72	-1.82	-0.04	-0.0435
100	-1.575	-1.68	-0.037	-0.0395
200	-1.515	-1.615	-0.036	-0.0390

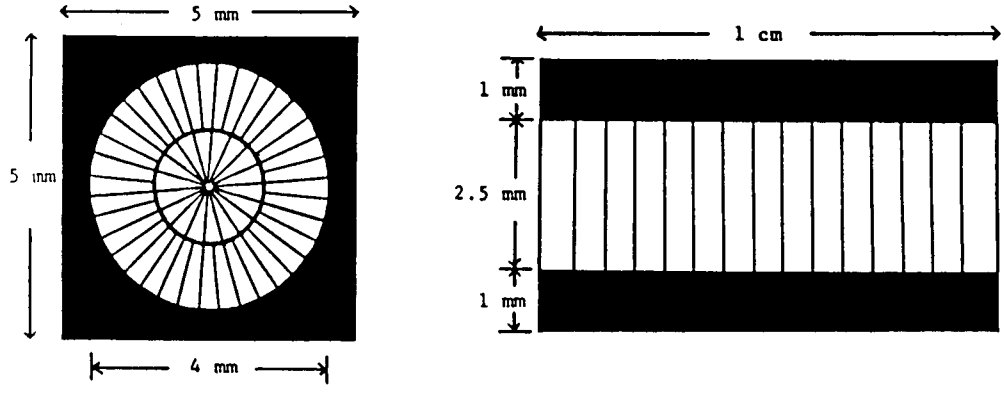

Circular Cell for
Cassegrainian Concentrator
100 AMO, 80°C

Rectangular Cell for
Slats Concentrator
20 AMO, 80°C

Figure 1. Geometries and Dimensions of the Concentrator Cells Modelled

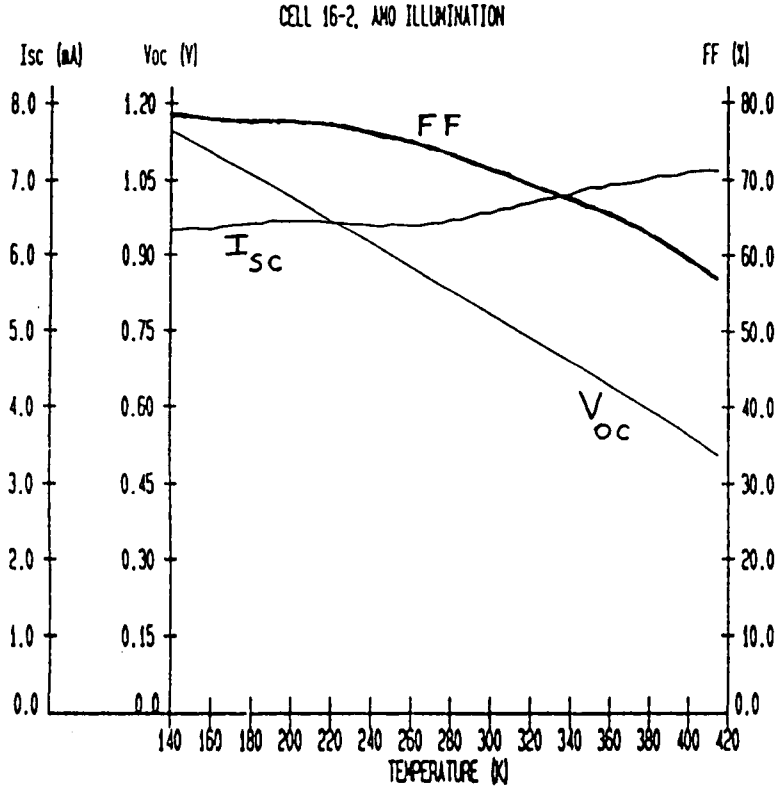

Figure 2.

Measured Variation of Performance Parameters with Temperature for One of Four InP Solar Cells

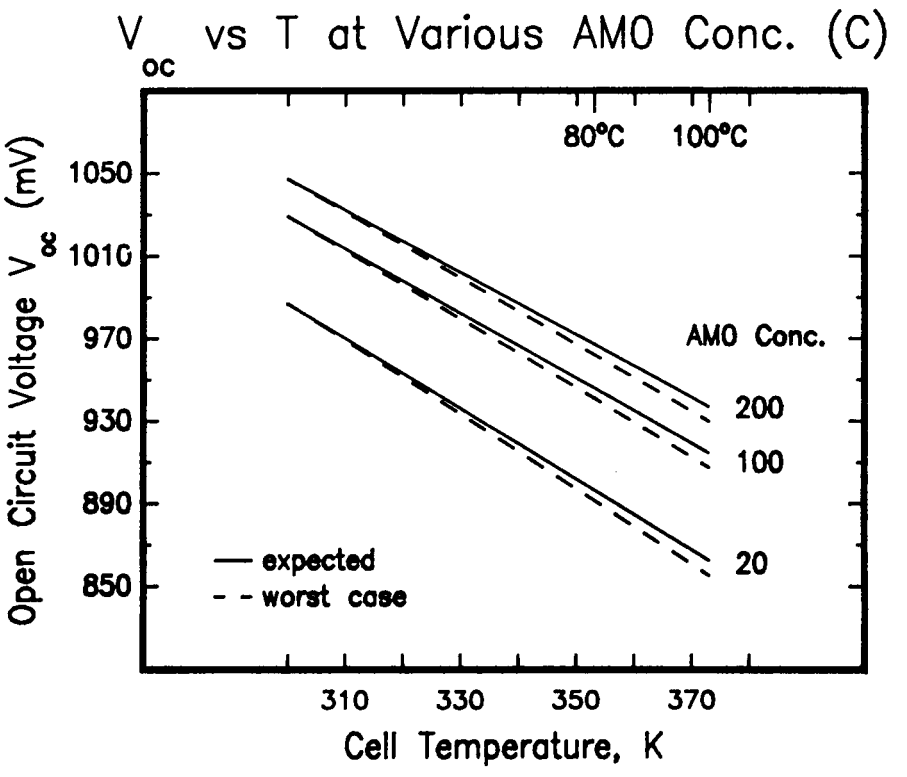

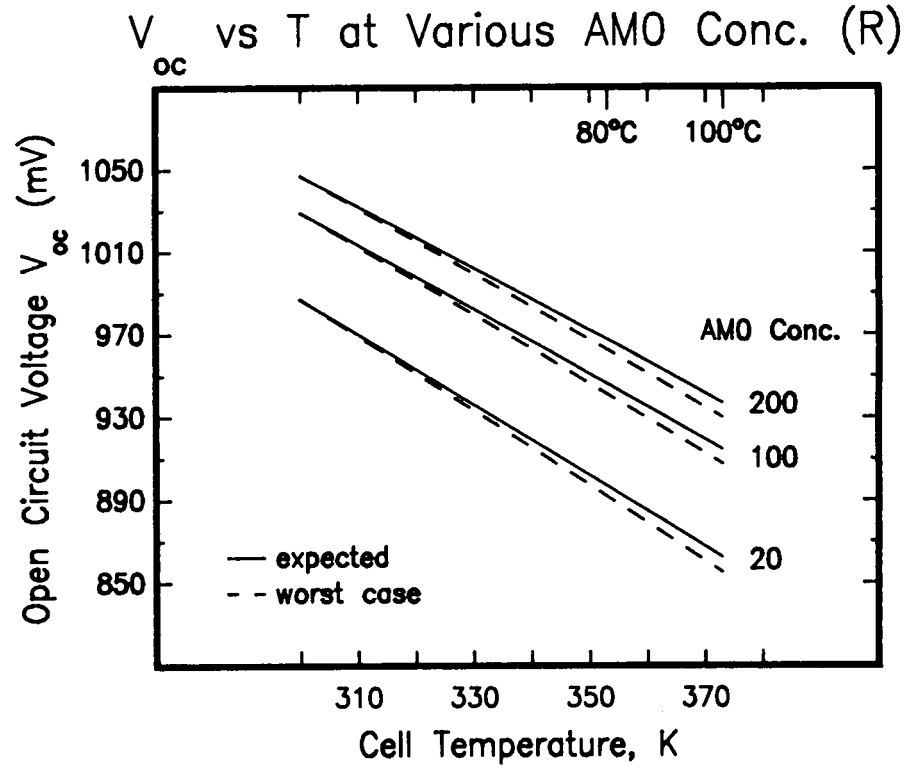

Figure 3. V_{oc} versus Temperature and AMO Concentrations for Circular (C) and Rectangular (R) Near-Optimum Cells

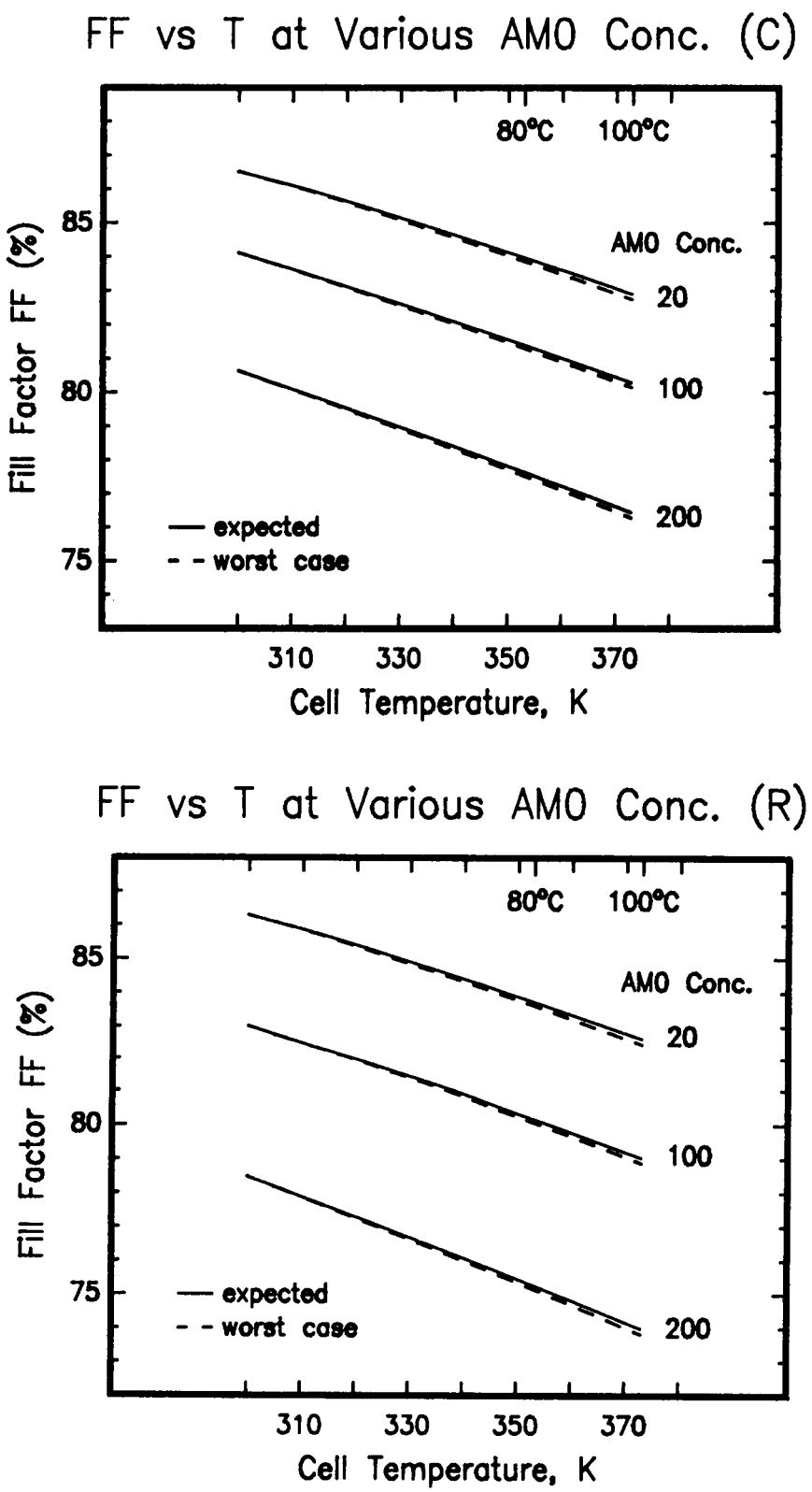

Figure 4. FF versus Temperature and AMO Concentrations for Cicrular (C) and Rectangular (R) Near-Optimum Cells

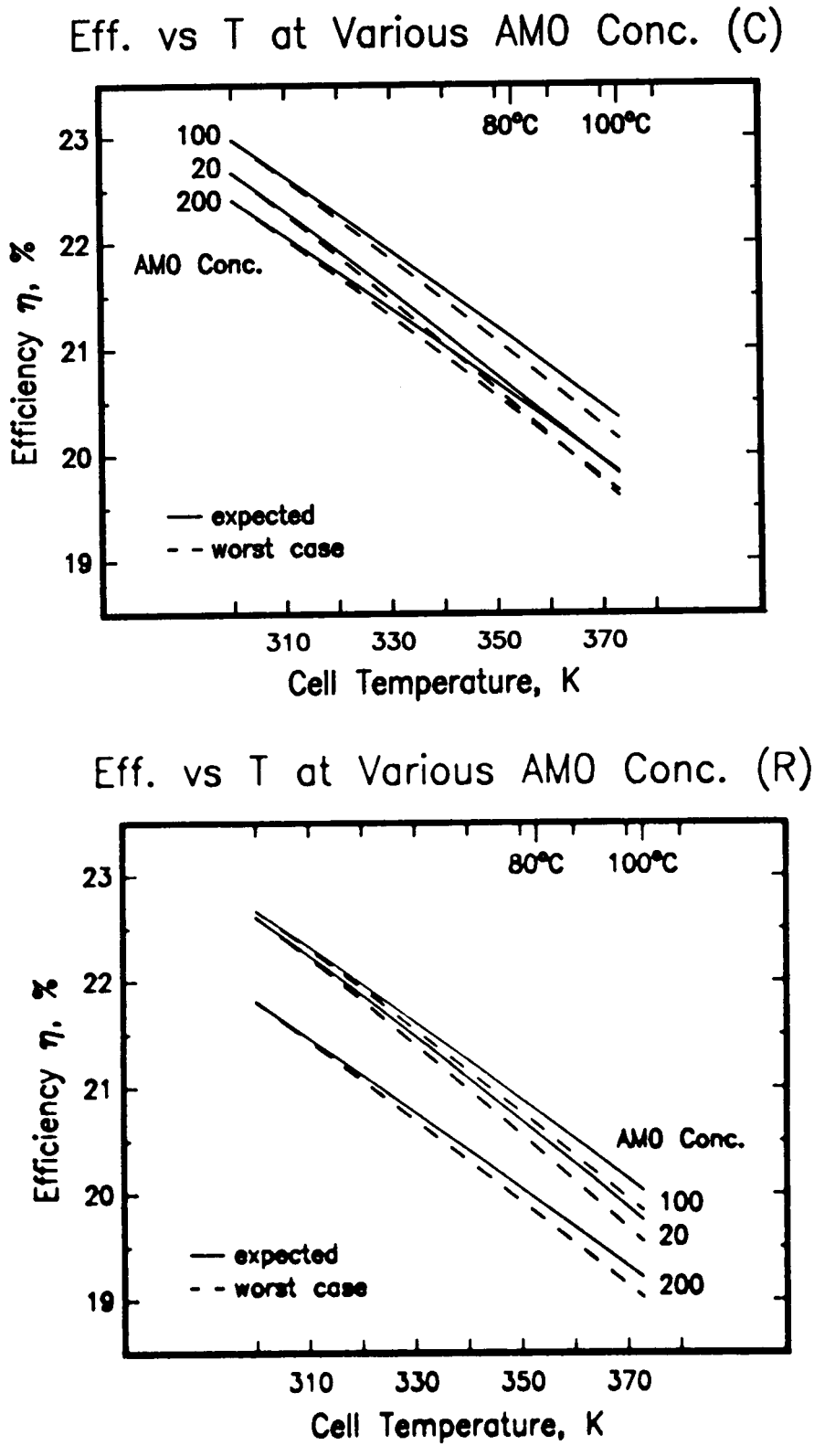

Figure 5. Efficiency versus Temperature and AMO Concentrations for Circular (C) and Rectangular (R) Near-Optimum Cells